# Catalyst Control over S(IV)-stereogenicity via Carbene-derived Sulfinyl Azolium Intermediates

Benpeng Li,[1,5+] Junyuan Hu,[6+] Minghong Liao,[1] Qin Xiong,[1] Yaqi Zhang,[1] Yonggui Robin Chi[1,2], Xinglong Zhang[3,4,*], Xingxing Wu[1,*]

[1]State Key Laboratory of Green Pesticide, Key Laboratory of Green Pesticide and Agricultural Bioengineering, Ministry of Education, Guizhou University, Huaxi District, Guiyang 550025, China.
[2]School of chemistry, chemical engineering, and biotechnology, Nanyang Technological University, Singapore 637371, Singapore
[3]Department of Chemistry, The Chinese University of Hong Kong, Shatin, New Territories, Hong Kong, China
[4]Institute of High Performance Computing, Agency for Science, Technology and Research (A*STAR), 1 Fusionopolis Way, #16-16, Connexis, Singapore 138632, Singapore
[5]School of Life and Health Science, Kaili University, Kaili 556011, China.
[6]Institute of Advanced Synthesis, School of Chemistry and Molecular Engineering, Jiangsu National Synergetic Innovation Center for Advanced Materials, Nanjing Tech University, Nanjing 211816, China.

[+] These authors contributed equally to this work
*Corresponding author. Email: wuxx@gzu.edu.cn; zhang_xinglong@ihpc.a-star.edu.sg

# 3. Computational section

## 3.1 Conformational sampling

Conformational sampling of key reaction intermediates and transition states was carried out at GFN2-xTB[16–18] level of theory using the CREST program version 2.12 by Grimme and co-workers.[19,20] The conformers and rotamers ensemble was generated using the iterative metadynamics based on genetic z-matrix crossing algorithm (iMTD-GC). Conformers were further optimized at GFN2-xTB level with very tight (*-opt vtight*) optimization. We then further chose 10 of the lowest energy conformers from each CREST sampling result to be further optimized at density functional theory (DFT) level of theory and used the conformer of the lowest DFT energy for full mechanistic studies and final potential energy surface (PES) Gibbs energy profile.

## 3.2 Density functional theory (DFT) calculations

DFT calculations were carried out using the *Gaussian 16* rev. B.01 program.[21] The global hybrid functional M06-2X[22] with the def2-SVPD[23,24] Karlsruhe-family basis set for S and I atoms and def2-SVP[23,25] basis set for all other atoms (this mixed basis set is denoted BS1) was employed for all gas-phase optimizations. The "D" in def2-SVPD basis set denotes diffuse functions which are important for the correct description of anionic electron distributions.[26–28] The M06-2X functional was chosen for the study of present system, as it has been employed in the studies of NHC organocatalysis with good accuracy.[29–35] Minima and transition structures on the potential energy surface (PES) were confirmed as such by harmonic frequency analysis, showing respectively zero and one imaginary frequency, at the same level of theory. Intrinsic reaction coordinate (IRC) analyses[36,37] were performed to confirm that the found TSs connect to the right reactants and products.

Single point (SP) corrections were performed using M06-2X functional with def2-TZVPD[23,24] basis set for S and I atoms and def2-TZVP[23,25] for all other atoms (denoted BS2). The integral equation formalism variant of the polarizable continuum model (IEF-PCM) with the SMD implicit continuum solvation model[40] was included to account for the solvent effect of toluene. Gibbs energies were evaluated at –60ºC

temperature (reaction condition), using the entropic quasi-harmonic treatment scheme of Grimme,[26] at a cut off frequency of 100 $cm^{-1}$. The free energies were further corrected using standard concentration of 1 mol/L, which was used in solvation calculations. The free energies reported in Gaussian from gas-phase optimisation were further corrected using standard concentration of 1 mol/L,[38–40] which were used in solvation calculations, instead of the gas-phase 1atm used by default in Gaussian program. Data analysis was carried out using the GoodVibes code version 3.1.1.[41] Gibbs energies evaluated at SMD (toluene)-M06-2X/BS2//M06-2X/BS1 level of theory are given in kcal/mol and used for discussion throughout. All molecular structures and molecular orbitals were visualized using *PyMOL* software.[42]

### 3.3 Model reaction

We chose the following reaction (entry 13, Scheme 1 of the main text) as our model system to study the catalytic mechanism of the NHC-catalyzed formation of chiral sulfoxide reaction (Scheme S37). From experimental evidence, we envisioned that substrates **1a** and **3a** will react to form mixed anhydride **IB**. From there, the chiral NHC may attack each of the enantiomer of **IB** to give epimers **IIB** and **IIB'**. We studied the detailed mechanisms of these steps computationally.

**Scheme S37.** Model reaction used for computational studies.

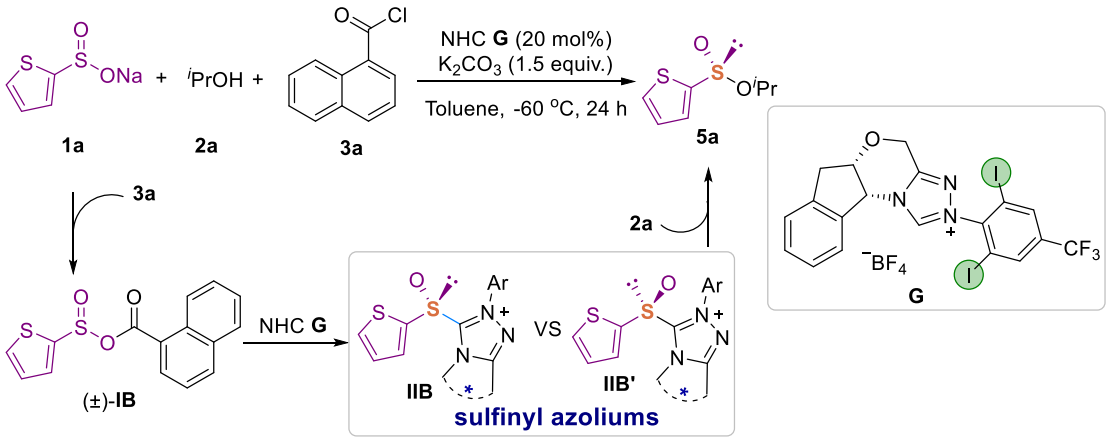


### 3.4 Racemization of mixed anhydride

We performed DFT calculations to understand if the mixed anhydride substrate, **IB**, may racemize under the reaction conditions. The mixed anhydride may undergo a trigonal planar transition state (TS), **TS_A**, that interconverts the two enantiomeric

forms of this substrate. However, this TS has a very high barrier of 62.1 kcal/mol, which is unfeasible at the reaction temperature of -60ºC. The mixed anhydride may also undergo a trigonal planar TS in the presence of the NHC catalyst, **TS_A'**. However, this has also very high barrier of 71.0 kcal/mol. The DFT optimized structure is shown in Figure S12.

| **TS_A** | **TS_A'** |
|---|---|
| $\Delta G^{\ddagger}$ = 62.1 | $\Delta G^{\ddagger}$ = 71.0 |
| 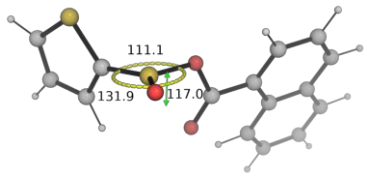 | 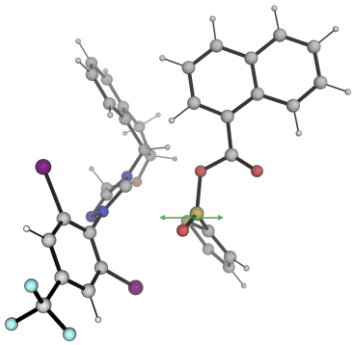 |
| **TS_B** | **TS_B'** |
| $\Delta G^{\ddagger}$ = 0.9 | $\Delta G^{\ddagger}$ = 0.9 |
| 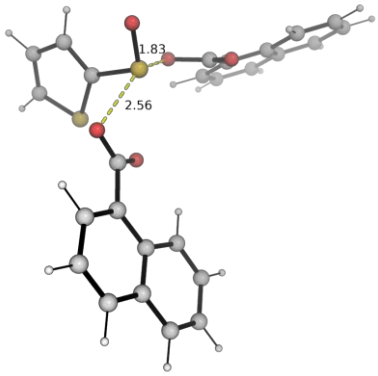 | 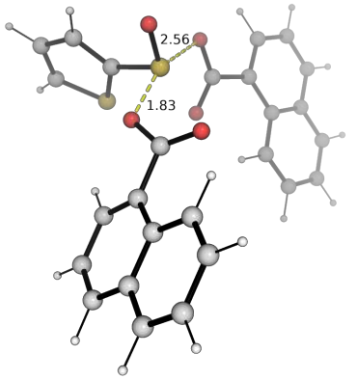 |

**Figure S12**. DFT-optimized structures of the transition states for the racemization of mixed anhydride. Key bond distances are given in Å and key angles are given in degrees. Green arrows indicate the vibrational mode for TSs. Activation barriers are in kcal/mol and taken relative to the mixed anhydride as zero reference.

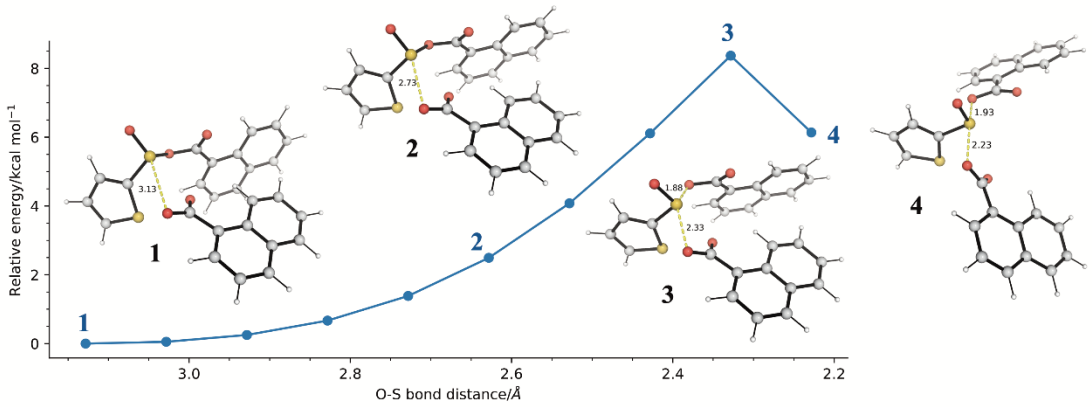


**Figure S13.** Relaxed potential energy surface (PES) scan along O–S distance in the gas phase.

We found that with the assistance of 1-naphthoate, the two enantiomers of the mixed anhydride **IB**, can racemize readily. An initial relaxed PES scan in the gas along the O(1-naphthoate)–S(mixed anhydride) distance shows that there exists a transition state for the formation of O–S bond between 1-naphthoate and the mixed anhydride, with an upper bound energy barrier of about 8 kcal/mol (Figure S13). Using the highest point on this scan as an initial guess for TS search, we located a TS for the attack of mixed anhydride S by 1-naphthoate, **TS_B**. The Gibbs energy profile for this process is shown in Figure S14. Key TS structures for this process are shown in Figure S12. The energy profile is symmetric: as the 1-naphthoate attacks the mixed anhydride, a stable intermediate **INT_B** is formed, before the other 1-naphthoate group leaves ($S_N2$ attack with inversion of configuration). From the Gibbs energy profile, we see that 1-naphthoate-assisted racemization of the mixed anhydride has a barrier of 3.5 kcal/mol in toluene solvent.

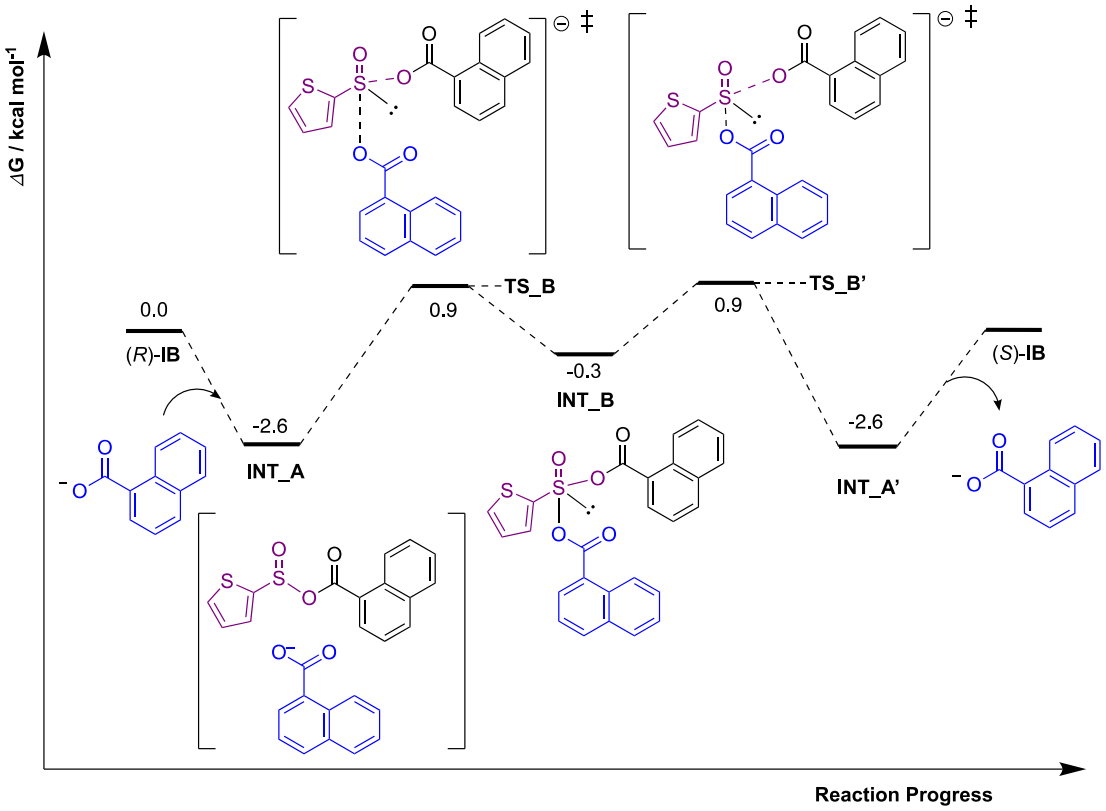


**Figure S14**. Gibbs energy profile for the 1-naphthoate-assisted racemization of mixed anhydride.

### 3.5 Formation of NHC-derived sulfinyl azolium intermediates

The feasibility of the attack of mixed anhydride by the chiral NHC catalyst was explored computationally. Initially, we performed a relaxed PES scan in the gas phase along the C(NHC)–S(mixed anhydride) bond distance to see if a transition state may be located. The NHC attacks the S atom of the mixed anhydride from the side of the lone pair, which is least sterically crowded. The relaxed PES scan energy profile is shown in Figure S15. Surprisingly, there is no transition state that can be found, as the energy rises (to a very high value, > 40 kcal/mol) as the C–S bond distance is shortened. However, if the NHC carbon attacks the sulfoxide S=O group from the other side, a TS is located successfully. This TS has a barrier of 35.6 kcal/mol if the NHC attacks *(R)*-mixed anhydride (**R_TS1'**, Figure S16) and a barrier of 38.1 kcal/mol if the NHC attacks *(S)*-mixed anhydride (**S_TS1'**, Figure S16). These barriers are quite high and indicate that the pathways via these transition states are not feasible at the reaction conditions (-60ºC).

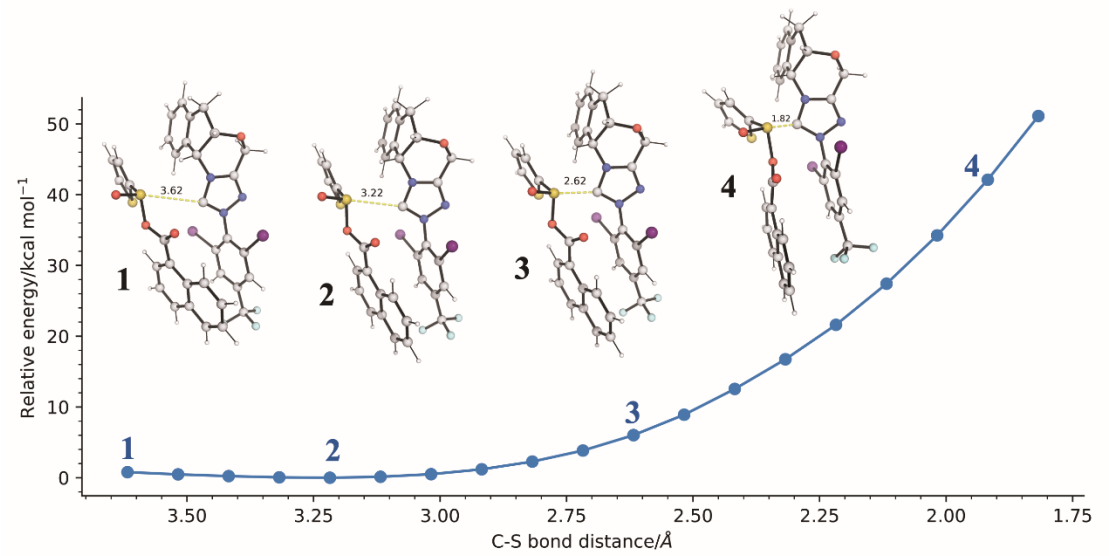


**Figure S15**. Relaxed potential energy surface (PES) scan along C–S distance in the gas phase where the NHC carbon attacks sulfoxide from the less hindered side.

Further TS searches allow us to locate trigonal bipyramidal TSs for the formation of NHC-derived sulfinyl azolium intermediates where the thiophene, S=O and the lone pair lie on a trigonal plane while the NHC carbon attacks the mixed anhydride and the 1-naphthoate group leaves (**R_TS1** and **S_TS1**, Figure S16). These TSs were verified by IRC studies. The species on either side of these TSs were also optimized. These indicate that the NHC-derived sulfinyl azolium intermediate can be formed (**R_INT2** with C–S distance of 1.89Å and **S_INT2** with C–S distance of 1.88Å).

| **R_TS1'** | **S_TS1'** |
|---|---|
| $\Delta G^{\ddagger}$ = 35.6 | $\Delta G^{\ddagger}$ = 38.1 |
| 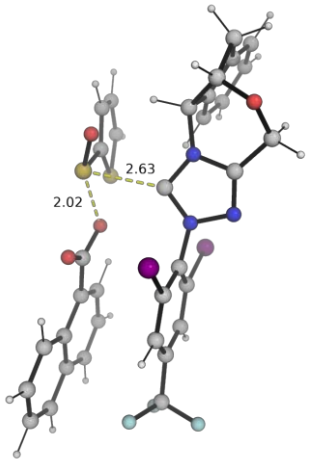 | 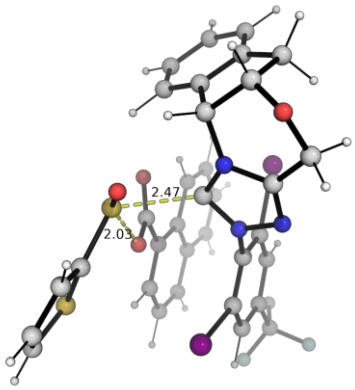 |
| **R_INT1** | **R_TS1** |

| ΔG = 3.8 | ΔG‡ = 12.2 |
|---|---|
| 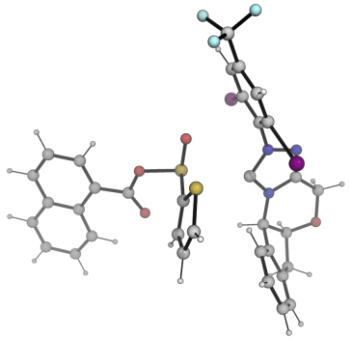 | 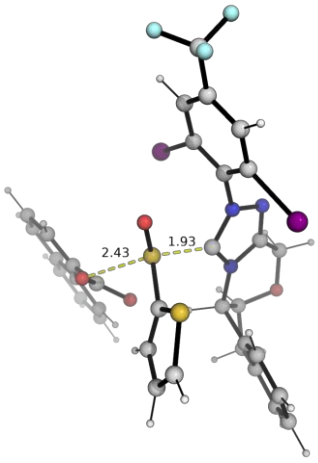 |
| **R_INT2** | **S_INT1** |
| ΔG = 8.4 | ΔG = 6.5 |
| 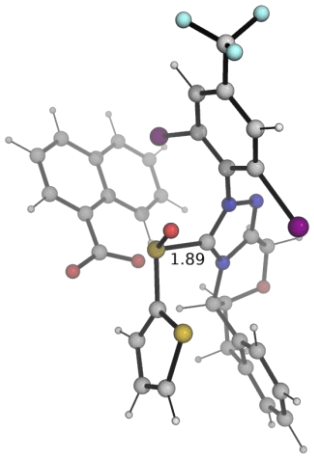 | 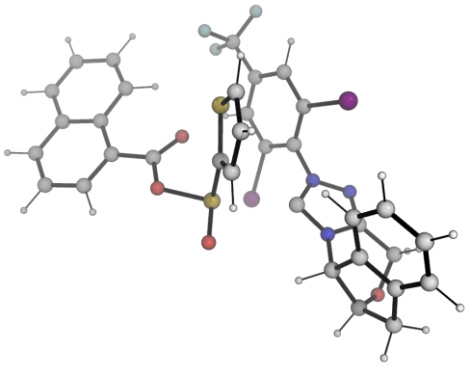 |
| **S_TS1** | **S_INT2** |
| ΔG‡ = 14.3 | ΔG = 8.8 |
| 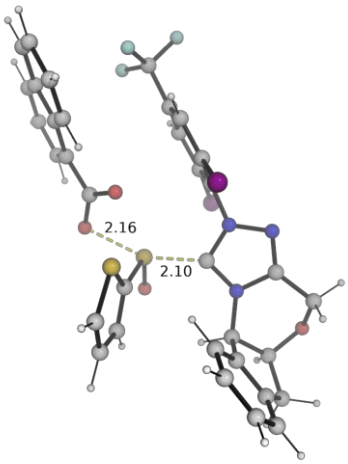 | 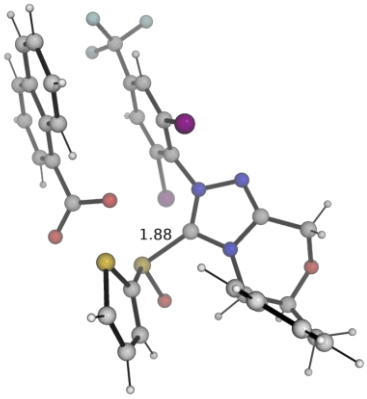 |

**Figure S16**. DFT-optimized structures of the lowest energy intermediates and transition states (TSs) for the formation of NHC-derived sulfinyl azolium species. Key

bond distances are given in Å. Activation barriers and energies are in kcal/mol and taken relative to the mixed anhydride as zero reference.

### 3.6 Racemization of NHC-derived sulfinyl azolium intermediate

The potential racemization process of the NHC-derived sulfinyl azolium intermediate was considered:

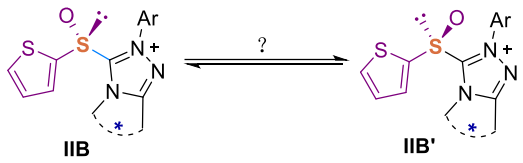


First, conformational samplings were performed and 10 of the lowest xTB energy conformers were optimized at DFT level. The lowest DFT energy conformer was then used for subsequent steps. Similar to the mixed anhydride, we found that this intermediate may racemize via a trigonal planar transition state (TS) structure, **TS_C** (Figure S17). However, this TS has a high barrier of 32.7 kcal/mol, indicating that this racemization process is not possible under the reaction conditions. In the presence of 1-naphthoate, the sulfinyl azolium intermediate may also undergo trigonal planar TS via **TS_D** (Figure S17), with a barrier of 48.2 kcal/mol. This is also too high to occur.

| TS_C | TS_D |
|---|---|
| $\Delta G^{\ddagger}$ = 32.7 | $\Delta G^{\ddagger}$ = 48.2 |

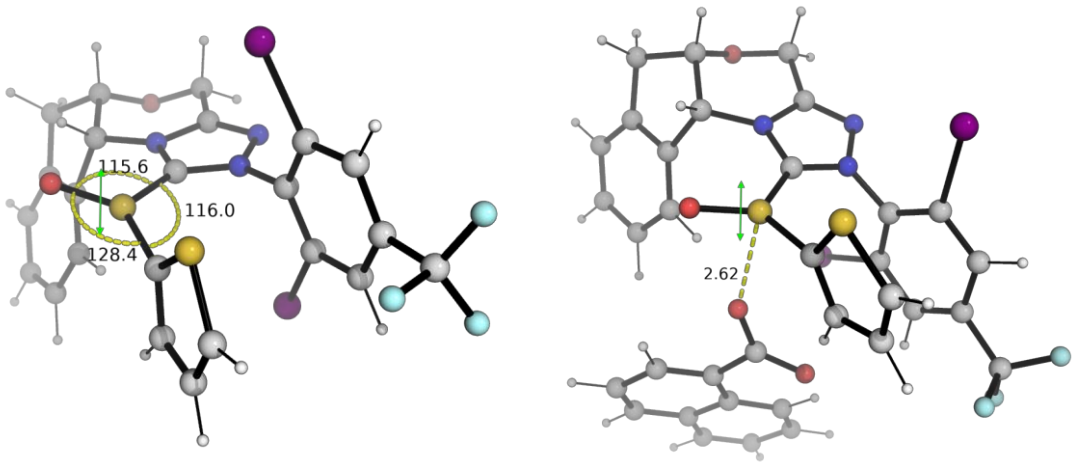


**Figure S17**. DFT-optimized structures of the transition states (TSs) for the racemization of NHC-derived sulfinyl azolium intermediate via trigonal pyramidal TSs. Key bond distances are given in Å and key angles are given in degrees. Green arrows

indicate the vibrational mode for the TSs. Activation barriers are in kcal/mol and taken relative to the mixed anhydride as zero reference.

We consider the case if the 1-naphthoate may assist in the isomerization of the sulfinyl azolium intermediate, similar to the case of mixed anhydride discussed in Figure S14. However, no such TS could be located (We used the located **TS_A** and modify it as a starting point for the TS search; *opt=modredundant* did not yield any imaginary frequency vibrational normal mode). We also consider the case if the sulfinyl azolium intermediate may undergo racemization with another molecule of NHC as the nucleophile attacking the S=O center. The relaxed PES scan is shown in Figure S18. This shows that as the carbene attacks the sulfinyl azolium intermediate, the barrier keeps increasing, such high barriers preclude the possibility of carbene-assisted racemization of the sulfinyl azolium intermediate.

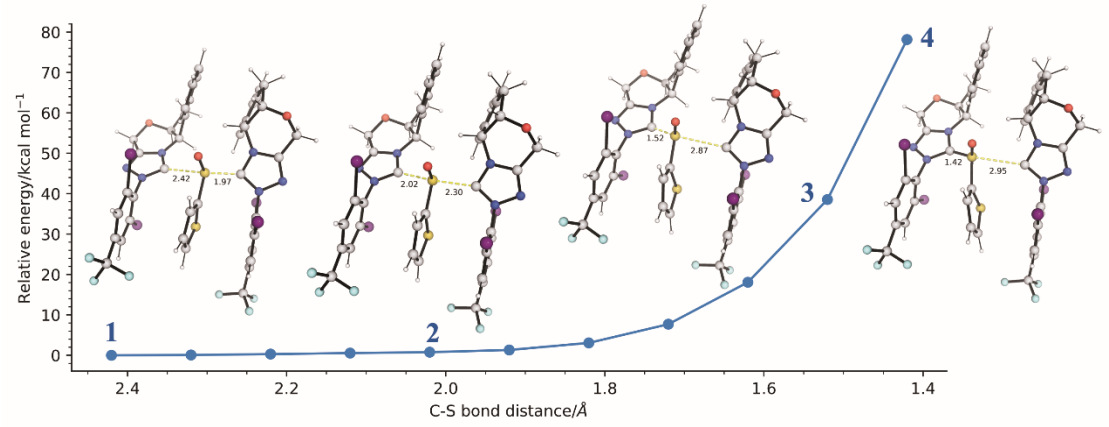


**Figure S18.** Relaxed potential energy surface (PES) scan along C–S distance in the gas phase where the NHC carbon attacks the NHC-derived sulfinyl azolium intermediate.

### 3.7 Product formation via nucleophilic attack on sulfinyl azolium intermediate

The nucleophilic attack on sulfinyl azolium intermediate by isopropanol was studied computationally. The DFT-optimized lowest energy TSs and their associated intermediates were shown in Figure S19.

| R_INT3 | R_TS2 |
|---|---|
| ΔG = 5.0 | $\Delta G^{\ddagger}$ = 9.5 |

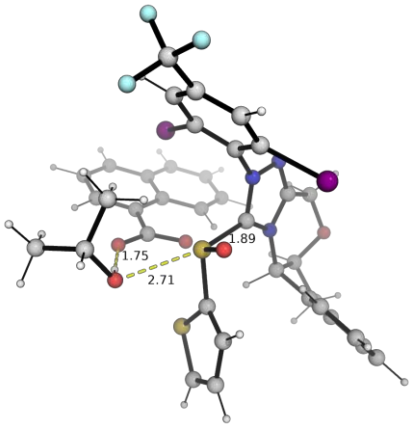


| R_INT4 |
|---|
| ΔG = -4.1 |

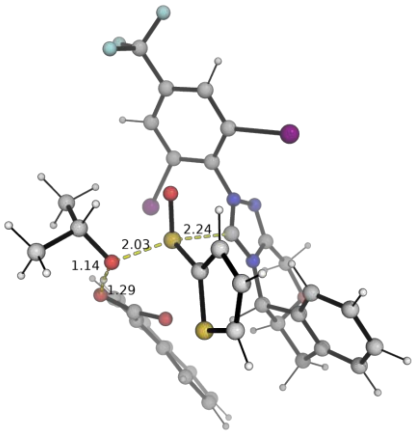


| S_INT3 |
|---|
| ΔG = 6.0 |

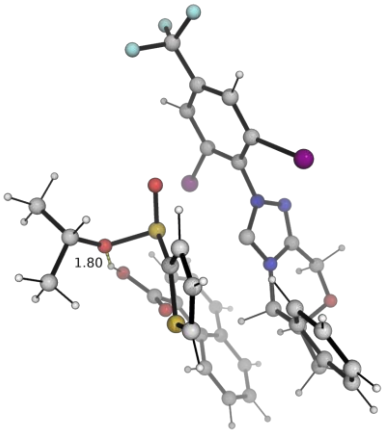


| S_TS2 |
|---|
| ΔG‡ = 9.9 |

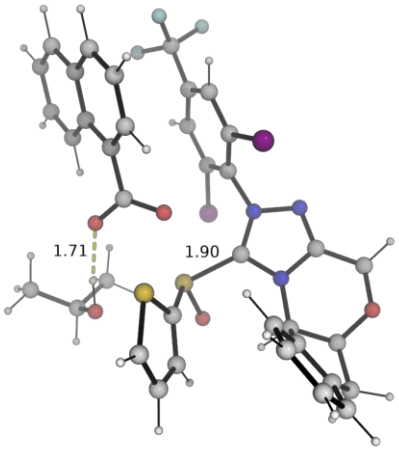


| S_INT4 |
|---|
| ΔG = -3.0 |

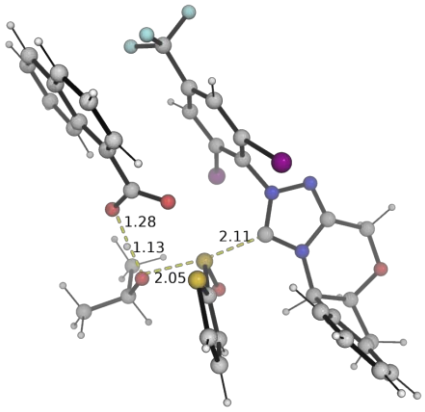


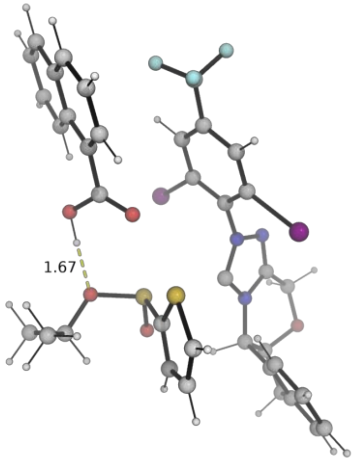


**Figure S19.** DFT-optimized structures of the lowest energy intermediates and transition states (TSs) for the product formation. Key bond distances are given in Å. Activation barriers and energies are in kcal/mol and taken relative to the mixed anhydride as zero reference.

### 3.8 Optimized structures and raw energy values

Geometries of all optimized structures (in .xyz format with their associated gas-phase energy in Hartrees) are included in a separate folder named *DFT_optimized_structures* with an associated readme.txt file. All these data have been uploaded to zenodo.org (https://zenodo.org/records/13120675).

Absolute values (in Hartrees) for SCF energy, zero-point vibrational energy (ZPE), enthalpy and quasi-harmonic Gibbs free energy for M06-2X/BS1 optimized structures and single point corrections in SMD(touluene) using M06-2X/BS2 functional are also included.

| Structures | E/au | ZPE/au | H/au | T.S/au | qh-G/au | SP SMD(toluene) M06-2X/BS2 |
|---|---|---|---|---|---|---|
| **NHC_G** | -1864.04018 | 0.284336 | -1863.7425 | 0.048226 | -1863.7871 | -1865.506322 |
| **naphthoic_acid** | -573.808928 | 0.164974 | -573.63813 | 0.027396 | -573.66499 | -574.461942 |
| **naphthoate** | -573.251 | 0.150743 | -573.09449 | 0.027326 | -573.121272 | -573.95539 |
| **mixed_anhydride** | -1598.446688 | 0.217065 | -1598.2199 | 0.038382 | -1598.256099 | -1599.648195 |
| **mixed_anhydride_c2** | -1598.444703 | 0.216976 | -1598.2179 | 0.038565 | -1598.254177 | -1599.647808 |
| **mixed_anhydride_c3** | -1598.446947 | 0.217162 | -1598.2201 | 0.037735 | -1598.255937 | -1599.647581 |
| **mixed_anhydride_c4** | -1598.444757 | 0.217165 | -1598.2179 | 0.037922 | -1598.253819 | -1599.646215 |
| **mixed_anhydride_c5** | -1598.445031 | 0.217156 | -1598.2182 | 0.037648 | -1598.253957 | -1599.645585 |
| **INT_A** | -2171.749932 | 0.369457 | -2171.365 | 0.050658 | -2171.412321 | -2173.625055 |

| | | | | | | |
|---|---|---|---|---|---|---|
| **TS_B** | -2171.741199 | 0.368902 | -2171.357 | 0.051627 | -2171.404676 | -2173.618324 |
| **INT_B** | -2171.743338 | 0.368859 | -2171.3585 | 0.054216 | -2171.407962 | -2173.619117 |
| **TS_B'** | -2171.741199 | 0.368902 | -2171.357 | 0.051627 | -2171.404677 | -2173.618324 |
| **INT_A'** | -2171.749932 | 0.369457 | -2171.365 | 0.050658 | -2171.412321 | -2173.625055 |
| **TS_A** | -1598.346333 | 0.215402 | -1598.1213 | 0.038179 | -1598.157277 | -1599.547653 |
| **TS_A'** | -3462.406912 | 0.500489 | -3461.8828 | 0.072747 | -3461.947797 | -3465.056839 |
| **TS_C** | -2889.041607 | 0.348664 | -2888.6759 | 0.055563 | -2888.727318 | -2891.079398 |
| **TS_D** | -3462.447152 | 0.501819 | -3461.9226 | 0.067582 | -3461.984817 | -3465.096299 |
| **IIB** | -2889.091214 | 0.349671 | -2888.7243 | 0.055905 | -2888.776118 | -2891.13233 |
| **IIB_c2** | -2889.08841 | 0.349807 | -2888.7213 | 0.056298 | -2888.773284 | -2891.129103 |
| **IIB_c3** | -2889.0869 | 0.349808 | -2888.7198 | 0.057173 | -2888.772069 | -2891.12631 |
| **IIB_c4** | -2889.086903 | 0.349867 | -2888.7197 | 0.056696 | -2888.771797 | -2891.126327 |
| **IIB_c5** | -2889.086835 | 0.349813 | -2888.7197 | 0.056803 | -2888.771824 | -2891.126168 |
| **IIB'** | -2889.092783 | 0.349798 | -2888.7256 | 0.056875 | -2888.777865 | -2891.131424 |
| **IIB'_c2** | -2889.09352 | 0.349815 | -2888.7264 | 0.056385 | -2888.778364 | -2891.130901 |
| **IIB'_c3** | -2889.093039 | 0.350091 | -2888.7259 | 0.054976 | -2888.777144 | -2891.131013 |
| **IIB'_c4** | -2889.086472 | 0.3498 | -2888.7194 | 0.056093 | -2888.771296 | -2891.127703 |
| **IIB'_c5** | -2889.089238 | 0.349774 | -2888.7223 | 0.055669 | -2888.773938 | -2891.127238 |
| **IIB'_c6** | -2889.085201 | 0.349782 | -2888.7182 | 0.05554 | -2888.769839 | -2891.124682 |
| **R_INT1** | -3462.513677 | 0.502261 | -3461.9879 | 0.073262 | -3462.053133 | -3465.165305 |
| **R_TS1** | -3462.501439 | 0.502241 | -3461.9763 | 0.069886 | -3462.039563 | -3465.15325 |
| **R_INT2** | -3462.51327 | 0.502878 | -3461.9872 | 0.069757 | -3462.050562 | -3465.160149 |
| **R_TS1_c2** | -3462.500904 | 0.502512 | -3461.9755 | 0.069726 | -3462.038717 | -3465.152531 |

| | | | | | | |
|---|---|---|---|---|---|---|
| **R_TS1_c3** | -3462.508379 | 0.502698 | -3461.9833 | 0.065772 | -3462.04443 | -3465.15235 |
| **S_INT1** | -3462.516698 | 0.502315 | -3461.9909 | 0.072132 | -3462.055452 | -3465.161715 |
| **S_TS1** | -3462.509338 | 0.502763 | -3461.9842 | 0.066462 | -3462.04557 | -3465.151808 |
| **S_INT2** | -3462.519609 | 0.503759 | -3461.9933 | 0.066084 | -3462.054682 | -3465.161682 |
| **S_TS1_c2** | -3462.496667 | 0.50208 | -3461.9716 | 0.070123 | -3462.034944 | -3465.14551 |
| **S_TS1'** | -3462.477995 | 0.502574 | -3461.953 | 0.066528 | -3462.014335 | -3465.113736 |
| **R_TS1'** | -3462.478562 | 0.502248 | -3461.9537 | 0.066773 | -3462.01537 | -3465.117339 |
| **R_INT3** | -3656.659922 | 0.613927 | -3656.0192 | 0.076826 | -3656.089062 | -3659.526379 |
| **R_TS2** | -3656.651806 | 0.610372 | -3656.0152 | 0.075765 | -3656.08411 | -3659.515945 |
| **R_TS2_c2** | -3656.651197 | 0.610187 | -3656.0148 | 0.075146 | -3656.083351 | -3659.513794 |
| **R_TS2_c3** | -3656.650742 | 0.610558 | -3656.0141 | 0.074735 | -3656.082474 | -3659.514122 |
| **R_TS2_c4** | -3656.650357 | 0.610927 | -3656.0133 | 0.074716 | -3656.081668 | -3659.514407 |
| **R_TS2_c5** | -3656.64948 | 0.609641 | -3656.0136 | 0.075575 | -3656.082323 | -3659.512238 |
| **R_TS2_c6** | -3656.650038 | 0.609757 | -3656.0141 | 0.074646 | -3656.08244 | -3659.512294 |
| **R_TS2_c7** | -3656.649269 | 0.609841 | -3656.0133 | 0.074509 | -3656.081616 | -3659.511889 |
| **R_TS2_c8** | -3656.648692 | 0.609367 | -3656.013 | 0.075544 | -3656.081841 | -3659.510563 |
| **R_TS2_c9** | -3656.648306 | 0.61134 | -3656.0109 | 0.07396 | -3656.078948 | -3659.511063 |
| **R_TS2_c10** | -3656.647533 | 0.609605 | -3656.0117 | 0.075209 | -3656.080361 | -3659.50886 |
| **R_TS2_c11** | -3656.646266 | 0.609278 | -3656.0107 | 0.075099 | -3656.079348 | -3659.508292 |
| **R_INT4** | -3656.670389 | 0.613764 | -3656.0296 | 0.079024 | -3656.100508 | -3659.539853 |
| **S_INT3** | -3656.660342 | 0.614088 | -3656.0198 | 0.074963 | -3656.088708 | -3659.525472 |
| **S_TS2** | -3656.653442 | 0.610443 | -3656.017 | 0.074077 | -3656.085032 | -3659.516058 |
| **S_TS2_c2** | -3656.65248 | 0.610349 | -3656.0159 | 0.076511 | -3656.085143 | -3659.514459 |

| | | | | | | |
|---|---|---|---|---|---|---|
| **S_TS2_c3** | -3656.654728 | 0.609594 | -3656.0189 | 0.074824 | -3656.087351 | -3659.514039 |
| **S_TS2_c4** | -3656.651727 | 0.609525 | -3656.016 | 0.074961 | -3656.084569 | -3659.513442 |
| **S_TS2_c5** | -3656.652082 | 0.609718 | -3656.0164 | 0.073951 | -3656.084359 | -3659.513908 |
| **S_INT4** | -3656.669391 | 0.613328 | -3656.029 | 0.078296 | -3656.09968 | -3659.537939 |

## 4.2 References

**Full reference for Gaussian software:**

Gaussian 16, Revision B.01, Frisch, M. J.; Trucks, G. W.; Schlegel, H. B.; Scuseria, G. E.; Robb, M. A.; Cheeseman, J. R.; Scalmani, G.; Barone, V.; Mennucci, B.; Petersson, G. A.; Nakatsuji, H.; Caricato, M.; Li, X.; Hratchian, H. P.; Izmaylov, A. F.; Bloino, J.; Zheng, G.; Sonnenberg, J. L.; Hada, M.; Ehara, M.; Toyota, K.; Fukuda, R.; Hasegawa, J.; Ishida, M.; Nakajima, T.; Honda, Y.; Kitao, O.; Nakai, H.; Vreven, T.; Montgomery Jr., J. A.; Peralta, J. E.; Ogliaro, F.; Bearpark, M.; Heyd, J. J.; Brothers, E.; Kudin, K. N.; Staroverov, V. N.; Kobayashi, R.; Normand, J.; Raghavachari, K.; Rendell, A.; Burant, J. C.; Iyengar, S. S.; Tomasi, J.; Cossi, M.; Rega, N.; Millam, J. M.; Klene, M.; Knox, J. E.; Cross, J. B.; Bakken, V.; Adamo, C.; Jaramillo, J.; Gomperts, R.; Stratmann, R. E.; Yazyev, O.; Austin, A. J.; Cammi, R.; Pomelli, C.; Ochterski, J. W.; Martin, R. L.; Morokuma, K.; Zakrzewski, V. G.; Voth, G. A.; Salvador, P.; Dannenberg, J. J.; Dapprich, S.; Daniels, A. D.; Farkas, Ö.; Foresman, J. B.; Ortiz, J. V; Cioslowski, J.; Fox, D. J. Gaussian, Inc., Wallingford CT, 2016.

1. Delany, E. G. ; Connon, S. J. Enantioselective N-heterocyclic carbene-catalysed intermolecular crossed benzoin condensations: improved catalyst design and the role of in situ racemisation. *Org. Biomol. Chem.* **2021**, *19*, 248–258.
2. Andreas, U. M.; Karolína, S.; Tomáš, S.; Burkhard, K. Eosin Y (EY) photoredox-catalyzed sulfonylation of alkenes: scope and mechanism. *Chem. Eur. J.* **2016**, *22*, 8381–8699.
3. Zhang, X.; Ang, E. C. X.; Yang, Z.; Kee, C. W.; Tan, C.-H. Synthesis of chiral sulfinate esters by asymmetric condensation. *Nature* **2022**, *604*, 298–303.
4. Huang, S.; Zeng, Z.; Zhang, N.; Qin, W.; Lan, Y.; Yan, H. Organocatalytic asymmetric deoxygenation of sulfones to access chiral sulfinyl compounds. *Nat. Chem.* **2023**, *15*, 185–193.
5. Liao, M.; Liu, Y.; Long, H.; Xiong, Q.; Lv, X.; Luo, Z.;Wu, X; Chi, R. C. Enantioselective sulfinylation of alcohols and amines by condensation with sulfinates. *Chem*. **2024**, *10*, 1541–1552.
6. Ye, X.; Moeljadi, A. M. P.; Chin, K. F.; Hirao, H.; Zong, L.; Tan, C. H. Enantioselective sulfoxidation catalyzed by a bisguanidinium diphosphatobisperoxotungstate ion pair. *Angew. Chem. Int. Ed.* **2016**, *128*, 7217–7221.

7. Su, F.; Lu, F.; Tang, K.; Lv, X.; Luo, Z.; Che, F.; Long, H.; Wu, X; Chi, Y. R. Organocatalytic C-H functionalization of simple alkanes. *Angew. Chem. Int. Ed.* **2023**, *135*, e202310072.
8. Ungureanu, A.; Levens, A.; Candish, L.; Lupton, D. W. N-heterocyclic carbene catalyzed synthesis of δ-sultones via α, β - unsaturated sulfonyl azolium intermediates. *Angew. Chem. Int. Ed.* **2015**, *127*, 11946–11950.
9. Lin, M.; Luo, J.; Xie, Y.; Du, G.; Cai, Z.; Dai, B.; He, L. SuFEx Reactions of sulfonyl fluorides, fluorosulfates, and sulfamoyl fluorides catalyzed by N-heterocyclic carbenes. *ACS Catal.* **2023**, *13*, 14503–14512.
10. Yuan, Y.; Han, Y.; Zhang, Z. K.; Sun, S.; Wu, K.; Yang, J.; Zhang, J. Enantioselective arylation of sulfenamides to access sulfilimines enabled by palladium catalysis. *Angew. Chem. Int. Ed.* **2024**, e202409541.
11. Cardinal-David, B.; Raup, D. E.; Scheidt, K. A. Cooperative N-heterocyclic carbene/Lewis acid catalysis for highly stereoselective annulation reactions with homoenolates. *J. Am. Chem. Soc.* **2010**, *132*, 5345–5347.
12. Chen, J.; Yuan, P.; Wang, L.; Huang, Y. Enantioselective β-protonation of enals via a shuttling strategy. *J. Am. Chem. Soc.* **2017**, *139*, 7045–7051.
13. Wu, Z.; Wang, J. Enantioselective medium-ring lactone synthesis through an NHC-catalyzed intramolecular desymmetrization of prochiral 1, 3-diols. *ACS Catal.* **2017**, *7*, 7647–7652.
14. Bera, S.; Samanta, R. C.; Daniliuc, C. G.; Studer, A. Asymmetric synthesis of highly substituted β-lactones through oxidative carbene catalysis with LiCl as cooperative lewis acid. *Angew. Chem. Int. Ed.* **2014**, *53*, 9622–9626.
15. Wang, M. H; Scheidt, K. A. Cooperative catalysis and activation with N-heterocyclic carbenes. *Angew. Chem. Int. Ed.*, **2016**, *55*, 14912–14922.
16. Bannwarth, C.; Ehlert, S.; Grimme, S. GFN2-XTB - an accurate and broadly parametrized self-consistent tight-binding quantum chemical method with multipole electrostatics and density-dependent dispersion contributions. *J. Chem. Theory Comput.* **2019**, *15*, 1652–1671.
17. Grimme, S.; Bannwarth, C.; Shushkov, P. A robust and accurate tight-binding quantum chemical method for structures, vibrational frequencies, and noncovalent interactions of large molecular systems parametrized for all spd-block elements (Z = 1-86). *J. Chem. Theory Comput.* **2017**, *13*, 1989–2009.

18. Bannwarth, C.; Caldeweyher, E.; Ehlert, S.; Hansen, A.; Pracht, P.; Seibert, J.; Spicher, S.; Grimme, S. Extended tight-binding quantum chemistry methods. *Wiley Interdiscip. Rev. Comput. Mol. Sci.* **2021**, *11*, e1493.
19. Grimme, S. Exploration of chemical compound, conformer, and reaction space with meta-dynamics simulations based on tight-Binding quantum chemical calculations. *J. Chem. Theory Comput.* **2019**, *15*, 2847–2862.
20. Pracht, P.; Bohle, F.; Grimme, S. Automated exploration of the low-energy chemical space with fast quantum chemical methods. *Phys. Chem. Chem. Phys.* **2020**, *22*, 7169–7192.
21. Frisch, M. J.; Trucks, G. W.; Schlegel, H. B.; Scuseria, G. E.; Robb, M. A.; Cheeseman, J. R.; Scalmani, G.; Barone, V.; Petersson, G. A.; Nakatsuji, H.; et al. Gaussian 16, Revision B.01. **2016**.
22. Zhao, Y.; Truhlar, D. G. The M06 suite of density functionals for main group thermochemistry, thermochemical kinetics, noncovalent interactions, excited states, and transition elements: two new functionals and systematic testing of four M06-class functionals and 12 Other function. *Theor. Chem. Acc.* **2008**, *120*, 215–241.
23. Weigend, F.; Ahlrichs, R. Balanced basis sets of split valence, triple zeta valence and quadruple zeta valence quality for H to Rn: design and assessment of accuracy. *Phys. Chem. Chem. Phys.* **2005**, *7*, 3297–3305.
24. Hellweg, A.; Rappoport, D. Development of new auxiliary basis functions of the karlsruhe segmented contracted basis sets including diffuse basis functions (Def2-SVPD, Def2-TZVPPD, and Def2-QVPPD) for RI-MP2 and RI-CC calculations. *Phys. Chem. Chem. Phys.* **2014**, *17*, 1010–1017.
25. Weigend, F. Accurate coulomb-fitting basis sets for H to Rn. *Phys. Chem. Chem. Phys.* **2006**, *8*, 1057–1065.
26. Davidson, E. R.; Feller, D. Basis set selection for molecular calculations. *Chem. Rev.* **1986**, *86*, 681–696.
27. Lynch, B. J.; Zhao, Y.; Truhlar, D. G. Effectiveness of diffuse basis functions for calculating relative energies by density functional theory. *J. Phys. Chem. A* **2003**, *107*, 1384–1388.
28. Papajak, E.; Zheng, J.; Xu, X.; Leverentz, H. R.; Truhlar, D. G. Perspectives on basis sets beautiful: seasonal plantings of diffuse basis functions. *J. Chem. Theory Comput.* **2011**, *7*, 3027–3034.

29. Yang, X.; Xie, Y.; Xu, J.; Ren, S.; Mondal, B.; Zhou, L.; Tian, W.; Zhang, X.; Hao, L.; Jin, Z.; Chi, Y. R. Carbene-catalyzed activation of remote nitrogen atoms of (Benz)imidazole-derived aldimines for enantioselective synthesis of heterocycles. *Angew. Chem. Int. Ed.* **2021**, *60*, 7906–7912.
30. Song, R.; Liu, Y.; Majhi, P. K.; Ng, P. R.; Hao, L.; Xu, J.; Tian, W.; Zhang, L.; Liu, H.; Zhang, X.; Chi, Y. R. Enantioselective modification of sulfonamides and sulfonamide-containing drugs: via carbene organic catalysis. *Org. Chem. Front.* **2021**, *8*, 2413–2419.
31. Lv, Y.; Luo, G.; Liu, Q.; Jin, Z.; Zhang, X.; Chi, Y. R. Catalytic atroposelective synthesis of axially chiral Benzonitriles via chirality control during bond dissociation and CN group formation. *Nat. Commun.* **2022**, *13*, 1–9.
32. Deng, R.; Wu, S.; Mou, C.; Liu, J.; Zheng, P.; Zhang, X.; Chi, Y. R. Carbene-catalyzed enantioselective sulfonylation of enone aryl aldehydes: a new mode of Breslow intermediate oxidation. *J. Am. Chem. Soc.* **2022**, *144*, 5441–5449.
33. Lv, W. X.; Chen, H.; Zhang, X.; Ho, C. C.; Liu, Y.; Wu, S.; Wang, H.; Jin, Z.; Chi, Y. R. Programmable selective acylation of saccharides mediated by carbene and boronic acid. *Chem* **2022**, *8*, 1518–1534.
34. Yang, X.; Wei, L.; Wu, Y.; Zhou, L.; Zhang, X.; Chi, Y. R. Atroposelective access to 1,3-oxazepine-containing bridged biaryls via carbene-catalyzed desymmetrization of imines. *Angew. Chem. Int. Ed.* **2022**, *62*, e202211977.
35. Luo, Z.; Liao, M.; Li, W.; Zhao, S.; Tang, K.; Zheng, P.; Chi, Y. R.; Zhang, X.; Wu, X. Ionic hydrogen bond-assisted catalytic construction of bitrogen stereogenic center via formal desymmetrization of remote diols. *Angew. Chem. Int. Ed.* **2024**, e202404979.
36. Fukui, K. Formulation of the reaction coordinate. *J. Phys. Chem.* **2005**, *7*, 4161–4163.
37. Fukui, K. The path of chemical reactions - the IRC approach. *Acc. Chem. Res.* **1981**, *14*, 363–368.
38. Bryantsev, V. S.; Diallo, M. S.; Goddard Iii, W. A.; Goddard, W. A. Calculation of solvation free energies of charged solutes using mixed cluster/continuum models. *J. Phys. Chem. B.* **2008**, *112*, 9709–9719.
39. Boyle, B. T.; Levy, J. N.; de Lescure, L.; Paton, R. S.; McNally, A. Halogenation of the 3-position of pyridines through zincke imine intermediates. *Science* **2022**, *378*, 773–779.

40. Darù, A.; Hu, X.; Harvey, J. N. Iron-catalyzed reductive coupling of alkyl iodides with alkynes to yield cis-olefins: mechanistic insights from computation. *ACS Omega* **2020**, *5*, 1586–1594.
41. Luchini, G.; Alegre-Requena, J. V.; Funes-Ardoiz, I.; Paton, R. S. GoodVibes: automated thermochemistry for heterogeneous computational chemistry data. *F1000Research* **2020**, *9*, 291.
42. Schrödinger, L. The PyMOL molecular graphics development component, version 1.8; **2015.**